

DEMOCRATIC DECAY

Andrey M. SHIROKOV *

Institute for Nuclear Physics, Moscow State University,

Moscow 119899, Russia

E-mail: shirokov@compnet.msu.su

Abstract

Results of some recent investigations of democratic three-body decays of nuclear systems are discussed. In particular, we consider experimental studies of three-body ($\alpha + N + N$)-decay of $A = 6$ nuclei and J -matrix calculations of monopole excitations in ^{12}C and $E1$ transitions in ^{11}Li in the three-body-continuum cluster models $\alpha + \alpha + \alpha$ and $^9\text{Li} + n + n$, respectively.

1. Introduction

Investigation of the decay properties of nuclear resonant states is an important part of the nuclear structure studies. Usually in such investigations only two-body decay channels are allowed for. Three-body decays are much more informative than the two-body ones, but the full description of a three-body decay is a very complicated problem. Thus it is very important to derive simple but accurate approximate approaches for the analysis of the experimental data and for making reliable theoretical predictions. One of the approaches of such kind is the approach based on the democratic decay approximation.

A three-body continuum spectrum wave function in the asymptotic region is generally a superposition of the components describing two- and three-body decay channels ¹. The democratic decay approximation accounts for the three-body channel only; two-body channels associated with the appearance of bound two-body subsystems and 'non-democratic' subdivision of the system of the type (2+1), are not allowed for in the approximation. Therefore, this approximation is valid only for the study of a three-body system in the case when all two-body decay channels are closed and the only open channel is a three-body channel. Generally speaking, if the three-body channel is the only open one, than the system can have two types of

*A talk presented at the conference Perspectives of Nuclear Physics in the Late Nineties (Hanoi, March 1994).

asymptotics¹. One of the asymptotics corresponds to the situation when one of the particles is scattered by another one and the third particle is a spectator. From the general physical point of view, this asymptotics is supposed to be of little importance for a nuclear system excited in some nuclear reaction and decaying via a three-body channel. The alternative type of the asymptotics is a superposition of ingoing and outgoing six-dimensional spherical waves (or, equivalently, six-dimensional plane wave and ingoing or outgoing six-dimensional spherical wave) and corresponds to the situation when the decaying system emits (or/and absorbs) three particles from one and the same point in space. The version of the scattering theory that allows only for three-body asymptotics of this type is called true three-body scattering theory, or, alternatively, $3 \rightarrow 3$ scattering theory; the approximation based on the allowance for $3 \rightarrow 3$ scattering only in the examination of nuclear reactions is called democratic decay approximation.

Nuclear structure studies within the framework of democratic decay approximation have been started in 70th by Prof. R.I.Jibuti with collaborators. The reviews of the results obtained by the Tbilisi group can be found in refs.^{2,3}. Recently a considerable progress has been made in both theoretical and experimental studies of democratic decays. Below we shall briefly review some of the recent results. In particular, we shall discuss the results of experimental studies of democratic decays of $A = 6$ nuclei via the three-body channel $\alpha + N + N$, theoretical investigations of monopole excitations of ^{12}C nucleus in the cluster model $\alpha + \alpha + \alpha$ and ^{11}Li structure studies in the cluster model $^9\text{Li} + n + n$.

2. Democratic decay of $A = 6$ nuclei

Detailed experimental study of the three-body decay of $T = 1$, $J^\pi = 0^+$ and 2^+ states in ^6He , ^6Li and ^6Be nuclei has been performed by the group from Kurchatov Institute (see^{4,5} and references therein). The democratic decay concept has been for the first time experimentally tested in this investigation, and the democratic nature of the decay of these states via the only open channel $\alpha + N + N$ has been unambiguously demonstrated.

The wave function in the democratic decay approximation has the following asymptotics:

$$\Psi^- \sim \kappa^{-1/2} \left[(2\pi)^{-3} \exp(i\mathbf{r}_{ab}\mathbf{q}_{ab} + i\mathbf{r}_{ab,c}\mathbf{q}_{ab,c}) + F \frac{e^{-i\rho\kappa}}{\rho^{5/2}} \right] \chi_{SM_S}, \quad (1)$$

where the first term is a six-dimensional plane wave while the second one is an ingoing six-dimensional spherical wave; F is the $3 \rightarrow 3$ scattering amplitude; \mathbf{r}_{ab} and $\mathbf{r}_{ab,c}$ are Jacobi coordinates, and \mathbf{q}_{ab} and $\mathbf{q}_{ab,c}$ are associated canonically conjugated momenta; hyper-radius $\rho = (\mathbf{r}_{ab}^2 + \mathbf{r}_{ab,c}^2)^{1/2}$, and $\kappa = (\mathbf{q}_{ab}^2 + \mathbf{q}_{ab,c}^2)^{1/2} = (2mE)^{1/2}/\hbar$; E is the energy measured from the three-body breakup threshold; S and M_S are the total spin

of the system and its projection while χ_{SM_S} is the spin part of the wave function. It is natural to expand the decay amplitude F in hyperspherical harmonics $Y_\Gamma \equiv Y_{KLM_L}^\gamma$ and to couple the three-body orbital momentum L and the spin S into the total angular momentum J . As a result, for the decay amplitude F_{JM} of a resonant state with the total spin J and its projection M we have the following expression ^{3,6}:

$$F_{JM} = \sum_{\Gamma} f_{KLS}^\gamma \cdot \left[Y_{KLM_L}^\gamma \chi_{SM_S} \right]_{JM} . \quad (2)$$

In eq. (2), K is hypermomentum, the multi-index $\Gamma \equiv \{K, L, M_L, S, \gamma\}$ plays the role of a channel index for the $3 \rightarrow 3$ scattering, and the multi-index γ stands for the set of all additional quantum numbers labelling different channels with the same quantum numbers K, L, M_L, S . It is convenient to use the Yamanouchi symbol r and the Young scheme $[f]$ for γ if there are three identical particles in the final state; otherwise orbital momenta l_{ab} and $l_{ab,c}$ corresponding to Jacobi coordinates \mathbf{r}_{ab} and $\mathbf{r}_{ab,c}$ are usually used for γ .

Eq. (2) is a generalization of the usual angular momentum decomposition of a two-body scattering amplitude and can be formally applied to any three-body decay. Note, that hypermomentum K is not an integral of motion, and due to the two-body interactions components labelled by different values of K mix together in the wave function, so, partial amplitudes $f_\Gamma \equiv f_{KLS}^\gamma$ with various values of K are present in the expansion (2). For a two-body decay channel the expansion (2) is non-convergent; in the case when two-body subsystems of the decaying three-body system have sharp resonances, the convergence can appear to be very slow. If two-body subsystems of the three-body system have neither bound nor sharp resonant states, than the $3 \rightarrow 3$ scattering amplitude F_{JM} converges rapidly and only few terms play an important role in eq. (2). Thus only in the case of democratic decay of such system it is possible to extract partial amplitudes $f_\Gamma \equiv f_{KLS}^\gamma$ from the experimental data, i.e., to solve the problem that is somewhat similar to the problem of the spin assignment to a resonant state by the analysis of two-body scattering data.

The hyperspherical harmonics $Y_{KLM_L}^\gamma$ are functions of five angles in the formal six-dimensional momentum space $\{\mathbf{q}_{ab}, \mathbf{q}_{ab,c}\}$. One of the angles, $\vartheta = \arctan(q_{ab}/q_{ab,c})$, rules the energy distribution between two Jacobi coordinates. Therefore, in order to evaluate partial amplitudes f_{KLS}^γ , one should analyze energy spectra of emitted particles. The analysis of ref. ⁴ of the three-body decay ${}^6\text{Be}(0^+) \rightarrow \alpha + p + p$ will serve us as an example.

${}^6\text{Be}$ levels have been populated in the reaction ${}^6\text{Li}({}^3\text{He}, {}^3\text{H}){}^6\text{Be}$ at $E_{{}^3\text{He}} = 40$ MeV. ${}^3\text{H}$ has been detected in the coincidence with α and/or p from the decay ${}^6\text{Be} \rightarrow \alpha + p + p$. The detection of ${}^3\text{H}$ of appropriate energy made it possible to select the levels of interest. Taken from ref. ⁴ the spectrum of α -particles from the decay of the ${}^6\text{Be}$ 0^+ state in the beryllium rest frame is depicted on fig. 1. The peculiar form of the spectrum cannot be reproduced in the model of independent escape of the decay products (phase volume calculations), nor can it be reproduced in the

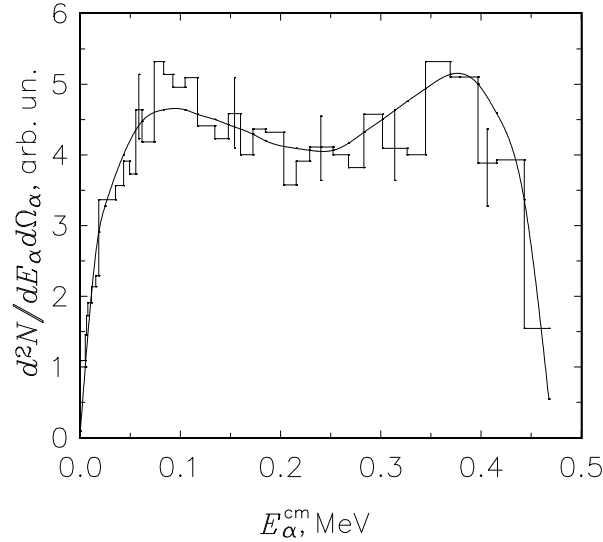


Figure 1: The α -particle spectrum (histogram) from ${}^6\text{Be}(0^+)$ decay in the beryllium rest frame. The solid line is the hyperspherical harmonics description of the data. The figure is taken from ref. ⁴.

model of sequential decay via the resonant states of p - p or α - p subsystems. At the same time, as is seen from fig. 1, the data are perfectly reproduced using expansion (2) and allowing only for the terms with $K = 0$ and 2. Nevertheless, the set of the partial amplitudes $\{f_{KLS}^\gamma\}$ cannot be uniquely determined from the analysis of the α -spectrum because various sets of $\{f_{KLS}^\gamma\}$ give the fit to the data of the same quality. One should involve in the analysis the energy spectrum of protons from the same reaction. The predictions for the proton spectrum obtained using various sets of $\{f_{KLS}^\gamma\}$ fitted to the α -spectrum, differ significantly. From the fit to both α - and p -spectra, the relative weights of $(6 \pm 5)\%$; $(44 \pm 12)\%$; and $(50 \pm 17)\%$ for the components $K = 0$; $K = 2$, $S = 0$; and $K = 2$, $S = 1$, respectively, have been obtained in ref. ⁴.

The set of partial amplitudes $\{f_{KLS}^\gamma\}$ can be used for the predictions of the kinematically complete experiment based on the triple-coincidence ${}^3\text{H} + p + \alpha$ measurements. As is seen from fig. 2, the set of $\{f_{KLS}^\gamma\}$ fitted to α - and p -spectra, perfectly matches the triple-coincidence data. Note, that the kinematical conditions of the triple-coincidence experiment ⁴ have been chosen in such a way, that the contribution of the $S = 1$ decay has been strongly suppressed. Therefore, the fine agreement between the theoretical curve and the experimental data on fig. 2 confirms the good quality of the determination of the relative weights of $K = 0$ and $K = 2$, $S = 0$

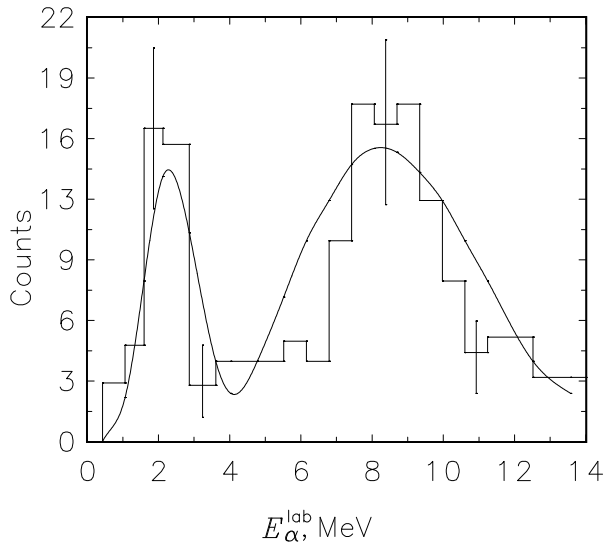


Figure 2: The histogram is the triple coincidence distribution measured in the kinematically complete experiment; the solid line is the prediction based on the α and proton spectra calculated using hyperspherical harmonics expansion. The figure is taken from ref. ⁴.

components only.

3. Democratic decay of 0^+ states in ^{12}C

In the previous section we have discussed the application of the democratic decay approximation to the analysis of experimental data. Now we shall discuss the use of the true three-body scattering theory in calculations.

It is well known that the giant monopole resonance generates a well-pronounced peak of the monopole excitation strength in heavy nuclei exhausting an essential fraction of the energy-weighted sum rule (EWSR). In light nuclei, the giant monopole resonance is very weak and exhausts, e.g., in ^{12}C , only $\sim 5\%$ of EWSR ⁷. However, the strong peak of $E0$ strength exhausting $\sim 90\%$ of EWSR has been predicted in various microscopic calculations (see, e.g., ref. ⁸). It has been shown in ref. ⁹ that this discrepancy should be attributed to the continuum spectrum effects, i.e., to the decay properties of the giant monopole resonance.

The 3α cluster model has been used in ref. ⁹. The ground state wave function has been obtained by diagonalization of the three-body Hamiltonian using the harmonic oscillator basis. For 0^+ continuum spectrum states only the decay channel $^{12}\text{C} \rightarrow$

$\alpha + \alpha + \alpha$ has been allowed for. This channel is the single open channel for low-lying 0^+ states and is supposed to dominate for 0^+ states with excitation energies of up to ~ 20 MeV. Continuum spectrum wave functions have been calculated by means of the oscillator representation of scattering theory (J -matrix method) ¹⁰ which had been generalized on the case of the true few-body scattering in ref. ¹¹.

In the J -matrix approach, the continuum spectrum wave function ψ_K^γ for a given three-body decay channel $\Gamma \equiv \{K, \gamma\}^\dagger$ is expressed as an infinite series expansion in six-dimensional harmonic oscillator functions φ_{nK} ,

$$\psi_K^\gamma = \sum_{n=0}^{\infty} D_{nK}^\gamma(E) \varphi_{nK}. \quad (3)$$

The basic approximation of the J -matrix approach is in neglecting potential energy matrix elements $V_{N\Gamma}^{N'\Gamma'} \equiv (V_{12} + V_{13} + V_{23})_{N\Gamma}^{N'\Gamma'}$ with a large number of oscillator quanta $N = 2n + K > \tilde{N}$ and/or $N' = 2n' + K' > \tilde{N}$; the infinite kinetic energy matrix T is not truncated. The exact wave functions of the Hamiltonian with the infinite kinetic energy matrix and truncated potential energy matrix for any positive energy E can be found by algebraic methods. To do it, one should first diagonalize the truncated Hamiltonian matrix, i.e., calculate its eigenvalues E_λ and corresponding eigenvectors $\zeta_{n\Gamma}^\lambda$. Next the matrix elements $\mathcal{P}_{n,\Gamma}^{n',\Gamma'}(E)$ of the matrix \mathcal{P} ,

$$\mathcal{P}_{n,\Gamma}^{n',\Gamma'}(E) = \sum_{\lambda} \frac{\zeta_{n'\Gamma'}^\lambda \zeta_{n\Gamma}^\lambda}{E_\lambda - E}, \quad (4)$$

are calculated. The $3 \rightarrow 3$ scattering S -matrix can be easily computed by the expression

$$S = (A^{(+)})^{-1} A^{(-)}, \quad (5)$$

where matrix elements of matrices $A^{(+)}$ and $A^{(-)}$,

$$A_{\Gamma\Gamma'}^{(\pm)} = \delta_{\Gamma\Gamma'} C_{\nu,K}^{(\pm)}(E) + \mathcal{P}_{\nu,\Gamma}^{\nu',\Gamma'}(E) T_{\nu',\nu'+1}^{\Gamma'} C_{\nu'+1,K'}^{(\pm)}(E); \quad (6)$$

$\nu = \frac{1}{2}(\tilde{N} - K)$ and $\nu' = \frac{1}{2}(\tilde{N} - K')$ are the truncation boundaries of the Hamiltonian matrix in the channels $\Gamma \equiv \{K, \gamma\}$ and $\Gamma' \equiv \{K', \gamma'\}$, respectively; the kinetic energy matrix elements $T_{n,n+1}^\Gamma = -\frac{1}{2}\hbar\omega \sqrt{(n+1)(n+K+3)}$; the eigenvectors $C_{n,K}^{(+)}(E)$ and $C_{n,K}^{(-)}(E)$ of the infinite kinetic energy matrix T can be easily calculated by analytical expressions or by recurrent relations (see ref. ¹¹ for details).

Finally, for the wave function with outgoing six-dimensional spherical wave in the channel Γ' and ingoing six-dimensional spherical waves in all allowed channels Γ ,

[†]Hereafter we shall omit the spin part of the wave functions and quantum numbers S , L , and M_L in the channel index $\Gamma \equiv \{K, L, M_L, S, \gamma\}$ and in the indexes of the functions used. In the case of spinless particles (e.g., α -particles), $S = 0$, L , and M_L are integrals of motion, therefore, all functions are labelled with the same values of S , L , and M_L and channels $\Gamma \equiv \{K, L, M_L, S, \gamma\}$ and $\Gamma' \equiv \{K', L', M_{L'}, S', \gamma'\}$ with $L \neq L'$ and/or $M \neq M_{L'}$ are not coupled.

the expansion coefficients $D_{n\Gamma}^{(\Gamma')}(E) \equiv D_{nK}^\gamma(E)$ [see eq. (3)] in the asymptotic region $n \geq \nu$ are calculated by the expression

$$D_{n\Gamma}^{(\Gamma')}(E) = \frac{1}{2} [\delta_{\Gamma\Gamma'} C_{nK}^{(+)}(E) - S_{\Gamma\Gamma'} C_{nK}^{(-)}(E)] , \quad (7)$$

while for calculation of $D_{n\Gamma}^{(\Gamma')}(E)$ in the interaction region $n \leq \nu$ the expression

$$D_{n\Gamma}^{(\Gamma')}(E) = - \sum_{\Gamma''} \mathcal{P}_{\nu''\Gamma''}^{n\Gamma}(E) T_{\nu'',\nu''+1}^{\Gamma''} D_{\nu''+1,\Gamma''}^{(\Gamma')}(E) \quad (8)$$

is used.

Ali-Bodmer $\alpha\alpha$ potential¹² has been used in ref.⁹; Coulomb interaction has been neglected. The truncation boundary $\tilde{N} = 18$ has been used in the calculations, i.e., the truncated Hamiltonian matrix accounted for all 3α oscillator states up to $18\hbar\omega$. The convergence for both the ground and continuum 0^+ states is achieved at $\tilde{N} \approx 18$ provided that $\hbar\omega = 10$ MeV. In the asymptotic region $n \geq \nu$ all channels Γ with $K \leq 10$ have been allowed for. However, in the interaction region $n \leq \nu$ we have accounted for all oscillator states up to $18\hbar\omega$, thus the hyperspherical harmonics with $K \leq 18$ have been allowed for in the interaction region. The inclusion of components with $K \geq 10$ in the channel space have not produced changes in the results.

The results of the calculations of ref.⁹ are presented on fig. 3. The solid line in fig. 3 represents the E -dependence of the $E0$ transition strength $F(E) = E |M_0|^2 / \sigma_\infty$ to the states above the $^{12}\text{C} \rightarrow 3\alpha$ threshold. Here, M_0 is the matrix element of the $E0$ transition from the ground state to the states with energy E . The dash-dotted curve displays the sum of the contributions to EWSR from all states with excitation energies less than E , i.e., the function

$$S(E) = \frac{\sigma(E)}{\sigma_\infty} \times 100\% , \quad (9)$$

where

$$\sigma(E) = \int_0^E E' |M_0|^2 dE' , \quad (10)$$

the monopole sum rule $\sigma_\infty \equiv \sigma(\infty) = \frac{2\hbar^2}{m} \langle R^2 \rangle_0$, and $(\langle R^2 \rangle_0)^{1/2}$ is the rms radius of the ^{12}C nucleus. The dashed step-like line is the plot of the function $S(E)$ calculated disregarding the effect of the 3α continuum. In this case, the height of each step is equal to the contribution to the EWSR from the corresponding quasistationary state obtained by the diagonalization of the truncated Hamiltonian matrix. It is seen that the most essential contributions to EWSR are connected with the quasistationary levels with excitation energies 6.11, 10.39, 13.60 and 22.30 MeV (31%, 29%, 13% and 13%, respectively). All the remaining levels with excitation energies up to 35 MeV exhaust about 7% of the EWSR.

The ^{12}C binding energy in calculations of ref.⁹ has been found to be $E_B = 7.27$ MeV (the experimental value is 7.27 MeV). The first excited 0^+ state with the

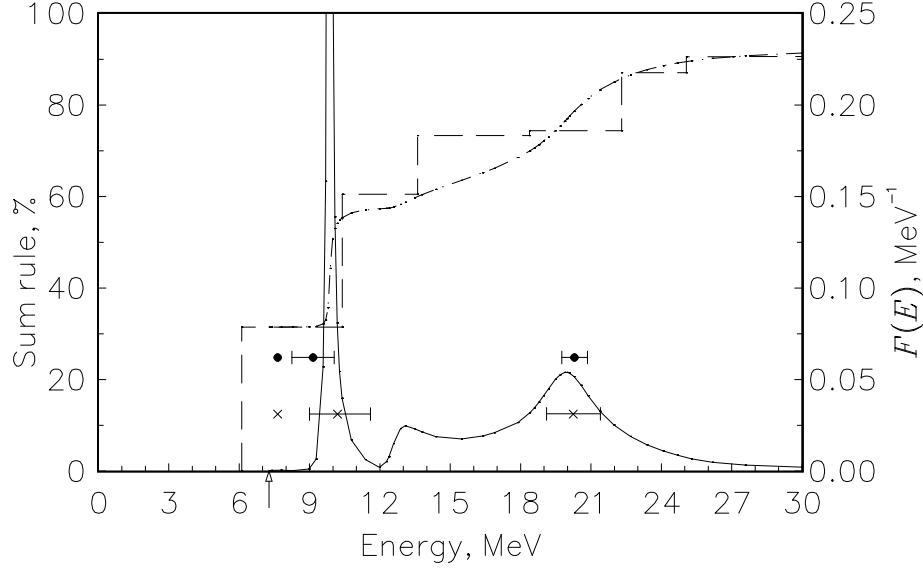


Figure 3: The solid line displays the monopole strength function $F(E) = E |M_0|^2 / \sigma_\infty$ for the states in continuum. The dash-dotted line is a plot of the function $S(E)$ [see eq. (9)], i.e., it displays the fraction of monopole EWSR exhausted by the states with excitation energies less than E . The dashed line is the same, but obtained by neglecting the effect of continuum. The experimental energies and the widths of the $E0$ resonances are indicated by crosses ⁷ and circles ¹³. The arrow indicates the $^{12}\text{C} \rightarrow 3\alpha$ reaction threshold. The figure is taken from ref. ⁹.

excitation energy $E_1 = 6.11$ MeV belongs to the discrete spectrum, so, the continuum does not affect its properties. The experimental value for E_1 is 7.66 MeV and this state belongs to the 3α continuum. However, its width is very small ($\Gamma = 9$ eV) and its properties are rather close to those of the discrete spectrum states.

The allowance for the continuum slightly changes the properties of the 10.39 MeV 0^+ state. Namely, the $F(E)$ maximum shifts down to $E = 9.9$ MeV, the state gets some width and its contribution to EWSR decreases to 26%.

However, in the 13–25 MeV excitation region the effect of the continuum appears to be essential. The levels in this excitation energy region get considerable widths and merge each other, forming very broad (of ~ 12 MeV in width) plateau of a peculiar shape, i.e., the strength function $F(E)$ is almost constant between 13 and 25 MeV except for a bump of the width of 2–3 MeV at an excitation energy of about 20 MeV. The bump should be related to the 20 MeV monopole resonance observed in refs. ^{13,7}. 33% of the EWSR is exhausted in the 12–26 MeV excitation energy region, with 16%

of the EWSR being exhausted in the 18–22 MeV interval.

The approach, as is seen from fig. 3, reproduces quite correctly the positions of the strong $E0$ absorption regions. The broad and smooth pedestal of the 20 MeV $E0$ excitation strength maximum can be easily misinterpreted in experimental studies as a background. The shape of the background that has been subtracted by Eyrich et al.⁷ in their study of the 20 MeV resonance, is similar to the shape of the pedestal on fig. 3. If the experimental background is a real manifestation of the smooth pedestal of the $E0$ strength, than it should be higher for small scattering angles. From fig. 3 of ref.⁷ it is seen, that the background is really enhanced at small angles. So, the experimental spectra of ref.⁷ is in qualitative agreement with theoretical results of ref.⁹. The further investigation of the nature of the background is needed.

The results presented on fig. 3 give the explanation why the giant monopole resonance is nearly not seen in ^{12}C . There are two physical reasons. First one is the strong fragmentation of the $E0$ strength in ^{12}C . As a result, more than 50% of the EWSR is exhausted by the 7.65 MeV and 10 MeV resonances, and not too much of the $E0$ strength is left for the giant monopole resonance. The second reason is the continuum spectrum effect. Due to the democratic decay, the giant monopole resonance gets a large width and merge with other 0^+ states. As a result, the $E0$ strength becomes very smooth, and the giant monopole resonance manifests itself only as a non-prominent bump on the smooth pedestal. About 15% of the EWSR is exhausted in the vicinity of 20 MeV bump, but if the pedestal is treated as a background, than the contribution of the resonance to the EWSR is severely underestimated.

4. ^{11}Li structure and the soft dipole mode

Light neutron-rich nuclei like ^6He , ^8He , ^{11}Li , ^{14}Be , etc., are extensively studied now (see recent review papers^{14,15} and references therein). These nuclei are often called exotic nuclei; they are also often called Barromean nuclei, because they have a well-pronounced cluster structure $\text{core} + n + n$ and after removing a neutron from any of these nuclei, the remaining system $\text{core} + n$ becomes unbound.[‡] Two excess loosely-bound neutrons have a wide spatial distribution with long tail reaching far out and form the so-called neutron halo. The neutron halo manifests itself in a number of unusual properties of exotic nuclei, in particular, in a large value of the rms radius of the nucleus, in the existence of the soft dipole mode, etc.

It is natural to make use of the democratic decay approximation in the study of Barromean nuclei. In ref.¹⁶, ^{11}Li has been studied in the cluster model $^9\text{Li} + n + n$. It has been shown in ref.¹⁶ that the democratic decay approximation within the framework of the J -matrix approach described in the previous section, is advantageous for the investigations not only of the continuum states, but of the ground state as

[‡]The heraldic symbol of the dukes of Barromeo is three rings connected in such a manner that after removing of any of the rings the two others become disconnected.

well.

In a usual variational calculation with the oscillator basis, it is impossible to describe the slowly-dying asymptotic tail of the halo neutron wave functions. In order to describe the neutron halo properties of the ^{11}Li nucleus, one is pushed to account for the oscillator states with a very large number of oscillator quanta. In the J -matrix approach, the infinite number of the oscillator states can be allowed for. For a bound state, the expansion coefficients $D_{n\Gamma}(E) \equiv D_{nK}^\gamma(E)$ [see eq. (3)] in the asymptotic region $n \geq \nu$ are of the form¹¹:

$$D_{n\Gamma}(E) = \alpha_\Gamma C_{nK}^{(+)}(E). \quad (11)$$

The bound state asymptotic normalization constants, α_Γ , are calculated by handling numerically the set of linear homogeneous equations¹¹

$$\sum_{\Gamma'} A_{\Gamma\Gamma'}^{(+)} \alpha_{\Gamma'} = 0. \quad (12)$$

Eq. (12) can be solved if only

$$\det A^{(+)} = 0. \quad (13)$$

Using eq. (13) the energy of a bound state can be easily calculated. This method of calculation of the bound state energies is equivalent to the location of the S -matrix pole¹¹ corresponding to the bound state, as is easily seen from eq. (5).

The expansion coefficients $D_{n\Gamma}(E) \equiv D_{nK}^\gamma(E)$ for the inner region $n \leq \nu$ are obtained using eq. (8). Finally, the wave function should be normalized.

The calculations¹⁶ have been performed using the shallow Gaussian n - ^9Li and n - n potentials of ref. ¹⁷. Only the states with the spin of the halo-neutron pair $S = 0$ have been considered. The three-body angular momentum of the ground state of ^{11}Li have been supposed to be equal to $L = 0$. The parameter $\hbar\omega = 7.1$ MeV has been used in the calculations. This value corresponds approximately to the minimum of the ground state energy E_0 .

The results for the ^{11}Li ground state for various values of the truncation parameter \tilde{N} are presented in the table 1. The variational ground state energies, $E_0^{(d)}$, obtained by the pure diagonalization of the truncated Hamiltonian matrix are listed in the second column, while the J -matrix results, E_0 , which are the solutions of the eq. (13) are listed in the third column. The values of the ^{11}Li r.m.s. radius, $\langle r^2 \rangle_{11}^{1/2 (d)}$ and $\langle r^2 \rangle_{11}^{1/2}$, obtained by the pure diagonalization of the truncated Hamiltonian matrix and with the allowance for the asymptotic tail of the wave function, respectively, are presented in the 4-th and the 5-th columns of the table. It is seen, that by locating the S -matrix pole using eq. (13) that is equivalent to the allowance for the long asymptotic tail of the wave function, the convergence of the ground state is essentially improved.

The results presented in the table 1 have been obtained using Lanczos smoothing of the three-body potential energy matrix¹⁸. The smoothing improves the convergency of calculations of the scattering characteristics. Nevertheless, the smoothing causes

Table 1: ^{11}Li ground state properties (see text for details).

Truncation boundary \tilde{N}	Ground state energy, MeV		Neutron halo mean square radius $\langle r^2 \rangle_{11}^{1/2}$, fm	
	$E_0^{(d)}$	E_0	$\langle r^2 \rangle_{11}^{1/2 (d)}$	$\langle r^2 \rangle_{11}^{1/2}$
12	-0.012	-0.150	2.83	3.31
16	-0.116	-0.199	2.91	3.29
20	-0.171	-0.225	2.98	3.31
24	-0.202	-0.240	3.04	3.32
Experiment	-0.247 ± 0.080		3.16 ± 0.11	

Table 2: The effect of the Lanczos smoothing on the ground state energy of ^{11}Li (see text for details).

\tilde{N}	10	12	14	16	18	20	22	24
E_0	-0.119	-0.150	-0.181	-0.199	-0.215	-0.225		-0.240
$E_0^{(w.s.)}$	-0.136	-0.266	-0.204	-0.262	-0.232	-0.262	-0.249	-0.263

the underestimation of the binding energy of a three-body system. The ^{11}Li ground state energy obtained in the J -matrix calculations without the use of the smoothing, $E_0^{(w.s.)}$, shows a staggering as \tilde{N} increases[§] (see table 2). $E_0^{(w.s.)}$ is seen to converge to the value of -0.263 MeV. The smoothing results in a usual-type monotonic decrease of E_0 as \tilde{N} increases, but $E_0^{(w.s.)} < E_0$ for all values of \tilde{N} . At the same time, the ground state wave functions obtained with the smoothing and without it, differ very slightly. So, below we shall discuss only the results of calculations with the smoothed potential energy matrix.

The quality of the convergence of the wave function in the J -matrix approach can be demonstrated by the plots of momentum distributions. Figure 4 presents the transverse momentum distribution of the cluster ^9Li in ^{11}Li that is currently supposed (the so-called Serber reaction mechanism) to be proportional to the ^9Li transverse momentum distribution $\frac{dN}{dp_\perp}$ in the fragmentation of high-energy ^{11}Li beams on target nuclei. The experimental data for ^{11}Li fragmentation¹⁹ are also presented on the figure. The results of J -matrix calculations with $\tilde{N} = 16$ and $\tilde{N} = 24$ are so close to each other that their plots on fig.4 coalesce and cannot be distinguished.

It is seen that in calculation of the ground state, the allowance for the wave function asymptotics is very important for a weakly-bound system like ^{11}Li . The terms of expansion (3) with the number of oscillator quanta $N \simeq 100$ that cannot be obtained in the usual oscillator-basis variational calculations, play an essential role in the formation of the transverse momentum distribution, r.m.s. radius, etc. The

[§]Note, that J -matrix calculation is not a variational one, so, the ground state energy may behave non-monotonically as \tilde{N} increases.

Figure 4: The ${}^9\text{Li}$ transverse momentum distribution in the ground state of ${}^{11}\text{Li}$. 1 — variational calculations, 2 — J -matrix calculations. Experimental data for the ${}^9\text{Li}$ transverse momentum distribution in the fragmentation of ${}^{11}\text{Li}$ 800 MeV/nucleon beam are taken from ref. ¹⁹.

convergence of $\langle r^2 \rangle_{11}^{1/2}$, transverse momentum distribution and other properties of the wave function (e.g., of the weights of its components) in the full J -matrix calculation is very good. Nevertheless, it is seen that the r.m.s. radius converges to a value that is somewhat larger than the experimental one, and the calculated transverse momentum distribution is narrower than the experimental one. These shortcomings can be overcome by the adjustment of n - ${}^9\text{Li}$ potential. We have not aimed to fit the potential to the ${}^{11}\text{Li}$ properties, we have just take its parameters from ref. ¹⁷. The differences between the calculated and experimental values of r.m.s. radius arise from the fact that in ref. ¹⁷ the potential has been fitted to the ${}^{11}\text{Li}$ r.m.s. radius and the binding energy in the *variational calculation* that is unable to reproduce these quantities with high accuracy.

The reduced probability of the $E1$ transition obtained in the cluster model, $\mathcal{B}(E1; E_f - E_0)$, is displayed on the figure 5. In the J -matrix approach, zero-width pure variational peaks of $\mathcal{B}(E1; E_f - E_0)$ gain finite widths and shift to lower energies. It is seen that in the calculation of $\mathcal{B}(E1; E_f - E_0)$ it is important to allow for the asymptotics not only for continuum states, but for the ground state as well. Due to the wide spatial distribution of the halo neutrons density, large distances contribute essentially to the $E1$ strength in the low-energy region. To account for this

Figure 5: Cluster $\mathcal{B}(E1; g.s. \rightarrow \text{continuum})$ in ^{11}Li . Zero-width peaks with diamonds on the top (1) given in arbitrary units, have been obtained in the pure variational approach for both the ground and excited states, i.e. the wave functions for the initial and the final states have been obtained by the diagonalization of the truncated Hamiltonian matrix. The curve with dots (2) has been calculated with the variational ground state wave function while the continuum spectrum wave function has been obtained by the J -matrix approach. The solid curve (3) is the result of J -matrix calculations for both the ground and continuum spectrum states.

contribution and to get a convergence, one should allow for the ground and continuum state wave function components with very large values of the total number of oscillator quanta $N \simeq 2000$ [¶] in calculations of $\mathcal{B}(E1; E_f - E_0)$. The large-distance $E1$ transitions enhance the peak of the cluster $\mathcal{B}(E1; E_f - E_0)$ and shift it to a lower energy. Obviously, this peak should be associated with the soft dipole mode. Thus, the neutron halo manifests itself in the appearance of the soft dipole mode that arises from the shift and enhancement of the $\mathcal{B}(E1; E_f - E_0)$ peak. This effect appears to be very important in the calculation of the ^{11}Li electromagnetic dissociation cross section (see below).

Large distances contribute essentially to $E2$ and $E0$ transitions, too. The shift and the enhancement of $\mathcal{B}(E0; E_f - E_0)$ and of $\mathcal{B}(E2; E_f - E_0)$ are even more pronounced. Nevertheless, $E2$ and $E0$ transitions do not play an important role in the electromagnetic dissociation, and we shall not discuss them here.

Figure 6 shows the comparison of the results of our calculations¹⁶ of the clus-

[¶]The classical turning point for the basis function with the total number of oscillator quanta $N = 1000$ is at a distance of ≈ 108 fm from the origin.

Figure 6: Comparison of our results¹⁶ for $\mathcal{B}(E1; g.s. \rightarrow \text{continuum})$ in ^{11}Li with results of other authors. 1 — J -matrix method¹⁶; 2 — ref. ²¹; 3 — ref. ²²; 4 — experimental data parametrization of ref. ²⁰.

ter $\mathcal{B}(E1; E_f - E_0)$ with the parametrization of experimental data of ref. ²⁰. The agreement is reasonable. The form of the $\mathcal{B}(E1; E_f - E_0)$ peak is well reproduced, the discrepancy in the position of the $\mathcal{B}(E1; E_f - E_0)$ maximum is supposed to be eliminated by the adjustment of the potentials. The results of the $\mathcal{B}(E1; E_f - E_0)$ calculations of refs. ^{21,22} are also depicted on fig. 6. The three-body cluster calculations with the allowance for democratic decay channels of ref. ²¹ performed using usual coordinate-space hyperspherical harmonics approach, nicely reproduce the energy of the soft dipole mode. Nevertheless, the form of the peak in our calculations is reproduced better. Note, that the authors of ref. ²¹ used another set of the potential parameters. The calculations of ref. ²² with the allowance for two-body decay channels only, failed to reproduce the form of the $\mathcal{B}(E1; E_f - E_0)$ peak and underestimate the energy of the soft dipole mode..

The soft dipole mode exhausts about 90% of the cluster EWSR, σ_∞^{clust} , associated with the excitation of the cluster degrees of freedom only. Nevertheless, it is easy to show that

$$\frac{\sigma_\infty^{clust}}{\sigma_\infty^{tot}} = \frac{1}{12} \approx 8.3\%, \quad (14)$$

where σ_∞^{tot} is the total EWSR accounting for excitations of all nucleons. So, the contribution from the soft dipole mode to the total EWSR is relatively small. In the

vicinity of the $\mathcal{B}(E1; E_f - E_0)$ maximum at the excitation energy $E \approx 1$ MeV only $\sim 8\%$ of the total EWSR is exhausted. Nevertheless, the account for the soft dipole mode results in an essential increase of the electromagnetic dissociation cross section of 0.8 GeV/nucleon ^{11}Li beams on Pb and Cu targets. The wide space distribution of the halo neutrons density is also well-manifested in the electromagnetic dissociation of ^{11}Li beam. The contribution of the large-distance $E\lambda$ -transitions to the cross section is about 50%. The calculations have been performed by the equivalent photon method. The only parameter of the method is the minimal value of the impact parameter b_{min} . We use for b_{min} the values of 9.0 fm for Pb and 6.8 fm for Cu target nuclei, respectively. These quantities are the sums of the ^{11}Li and target nucleus charge radii. With these values of b_{min} we obtain for the electromagnetic dissociation cross sections the values of 0.966 barn for the Pb target and 0.132 barn for the Cu target; the corresponding experimental values are 0.890 ± 0.110 barn and 0.21 ± 0.04 barn, respectively²³. $E0$ and $E2$ transitions give only 1.2% contribution in the cross sections.

Acknowledgments

I am thankful to Yu.A.Lurie, T.Ya.Mikhelashvili and Yu.F.Smirnov for a fruitful collaborate work some results of which have been discussed above. Valuable discussions with J.M.Bang, B.V.Danilin, R.I.Jibuti, I.J.Thompson and J.S.Vaagen are acknowledged.

This paper has been presented as a talk at the conference Perspectives of Nuclear Physics in the Late Nineties (Hanoi, March 1994). The support of my participation the conference by the International Science Foundation is acknowledged.

References

1. S.P.Merkuriev and L.D.Faddeev, *Quantum scattering theory for systems of few bodies* (Nauka Publishes, Moscow, 1985).
2. R.I.Jibuti, *Elem. Part. and Atom. Nucl.* **14** (1983) 741.
3. R.I.Jibuti and N.B. Krupennikova, *Hyperspherical harmonics method in quantum mechanics of few bodies* (Metsniereba, Tbilisi, 1984).
4. O.V.Bochkarev et al, *Nucl. Phys.* **A505** (1989) 215.
5. O.V.Bochkarev et al, *Yad. Phys. (Sov. J. Nucl. Phys.)* **55** (1992) 1729.
6. B.V.Danilin et al, *Yad. Phys. (Sov. J. Nucl. Phys.)* **46** (1987) 427.
7. W.Eyrich et al, *Phys. Rev.* **C36** (1987) 416.
8. V.V.Burov, V.N.Dostovalov, M.Kaschiev and K.V.Shitikova, *J. Phys.* **G7** (1981) 131.

9. T.Ya.Mikhelashvili, A.M.Shirokov and Yu.F.Smirnov, *J. Phys.* **G16** (1990) 1241.
10. H.A.Yamani and L.Fishman, *J. Math. Phys.* **16** (1975) 410; G.F.Filippov, *Yad. Phys. (Sov. J. Nucl. Phys.)* **33**(1981) 928; Yu.I.Nechaev and Yu.F.Smirnov, *Yad. Phys. (Sov. J. Nucl. Phys.)* **35** (1982) 1385.
11. Yu.F.Smirnov and A.M.Shirokov, *Preprint ITP-88-47P* (Kiev, 1988); A.M.Shirokov, Yu.F.Smirnov and S.A.Zaytsev, *to be published*.
12. S.Ali and A.Bodmer, *Nucl. Phys.* **80** (1966) 99.
13. D.Lebrun et al, *Phys. Lett.* **97B** (1980) 358.
14. C.A.Bertulani, F.L.Canto and M.H.Hussein, *Phys. Rep.* **226** (1993) 281.
15. Zhukov M.V. et al, *Phys. Rep.* **231** (1993) 151.
16. Yu.A.Lurie, A.M.Shirokov and Yu.F.Smirnov, *nucl-th/9407011*; *to be published*.
17. L.Johansen, A.S.Jensen and P.G.Hansen, *Phys. Lett.* **244B** (1990) 357.
18. J.Révai, M.Sotona and J.Žofka, *J. Phys.* **G11** (1985) 745; J.Mareš, *Czech. J. Phys.* **B37** (1987) 665.
19. T.Kobayashi et al, *Phys. Rev. Lett.* **60** (1988) 2599.
20. D.Sackett et al, *Preprint MSUCL* (Michigan State University, 1993).
21. B.V.Danilin, M.V.Zhukov, J.S.Vaagen, I.J.Thompson and J.M.Bang, *Preprint NORDITA – 93/34 N* (Copenhagen, 1994); *private communication*.
22. G.F.Bertsch and H.Esbensen, *Ann. of Phys.* **209** (1991) 327; H.Esbensen and G.F.Bertsch, *Nucl. Phys.* **A542** (1992) 310.
23. T.Kobayashi et al, *Phys. Lett.* **B232** (1989) 51.